PHYSICAL REVIEW A **75**, 010501(R) (2007)

Producing ultracold and trappable antihydrogen atoms

S. X. Hu*
Laboratory for Laser Energetics, University of Rochester, 250 East River Road, Rochester, New York 14623-1299, USA
(Received 10 August 2006; published 29 January 2007)

Both experiments and simulations have shown that the temperature of antihydrogen atoms ($\bar{H}$) formed in a strongly magnetized positron-antiproton plasma is mainly determined by the heavy particles' temperature. A routine to keep cooling antiprotons ($\bar{p}$) by using ultracold (<1 K) electrons is proposed under attainable experimental conditions. When cold positrons are loaded into such a low-temperature electron-antiproton mixture, ultracold antihydrogen atoms can be produced at a temperature below ~ 1 K. Our large-scale molecular-dynamics simulations, which involve 20 000 particles (e^-, e^+, and $\bar{p}$) evolving up to 1 μs, have confirmed the generation of trappable $\bar{H}$ atoms.

DOI: 10.1103/PhysRevA.75.010501 PACS number(s): 36.10.−k, 31.15.Qg, 34.80.Lx

Generating ultracold antihydrogen atoms ($\bar{H}$) that can be trapped in experiments is of fundamental importance for high-precision tests of both *CPT* violation and the gravitation between matter and antimatter [1]. Mixing antiprotons ($\bar{p}$) with positrons (e^+) in a nested Penning trap, experimentalists have created "cold" antihydrogen atoms in recent years [2]. Here, "cold" refers to cryogenic temperature of about a few kelvin. This significant progress has sparked an appreciable amount of both theoretical and experimental studies [3–9] on this important topic. The ultimate goal is that trappable $\bar{H}$ atoms can eventually be caught for high-precision spectroscopic measurements. In order to trap $\bar{H}$ atoms under current experimental conditions, it is essential that the formed antihydrogen atoms have to be "ultracold," at a temperature below ~ 1 K. Both experiments [9] and molecular-dynamics (MD) simulations [7,8] have shown that the $\bar{H}$ temperature is mainly determined by the initial temperature of antiprotons for current experimental situations; after all, antiprotons are the heavy particles in the mixture. Thus, cooling antiprotons down to very low temperatures is extremely crucial to the generation of trappable $\bar{H}$ atoms in experiments.

Electron cooling of $\bar{p}$ has proven to be an efficient way to slow down "hot" antiprotons [10]. Antiprotons can be brought into thermal equilibrium with the "coolant"—electrons (e^-); in this process the excess energy is emitted via cyclotron radiation of the latter. In recent years, techniques for making very-low-temperature electrons have been greatly advanced. A remarkable success showed that electrons in a Penning trap have been cooled down to 0.85 K through feedback cooling [11]. Although this technique was demonstrated for single-electron cooling, it may be possible to extend it for making low-density electrons as cold as ~ 0.5 K. Using such ultracold electron sources, one may expect to cool antiprotons further, to below ~ 1 K. If cold (4.2 K) positrons are loaded into such a low-temperature e^--$\bar{p}$ mixture, ultracold $\bar{H}$ atoms may be produced at a very low temperature. To fully explore this possibility, we have performed large-scale molecular-dynamics (MD) simulations with 20 000 particles (including e^+, e^-, and $\bar{p}$) evolving for up to 1 μs. Both positronium (Ps) and antihydrogen atoms are formed in such a strongly magnetized three-component plasma. Our simulation results indicate that a certain portion of $\bar{H}$ atoms are produced at a temperature below ~ 1 K. We anticipate that these ultracold antihydrogen atoms might be trapped with currently available techniques [12].

The electron cooling of antiprotons has been experimentally demonstrated [10]; in this process the antiproton energy can be dramatically lowered by several orders of magnitude. Since the time scale for such cooling is of the order of seconds or even longer, we cannot afford full MD simulations for the cooling process. Instead, we may properly assume that we have already obtained a low-temperature mixture of electrons and antiprotons. Such an e^--$\bar{p}$ mixture is schematically shown in the middle cylinder of Fig. 1, in which the small (green) balls represent electrons and the relatively large (red) balls stand for antiprotons. To simulate realistic experimental conditions, a constant magnetic field ($B=5.4$ T) is applied along the z axis of the cylinder. The cylinder has a radius of 100 μm and a length of 650 μm, inside which 2000 e^- and 2000 $\bar{p}$ are randomly placed. This gives a particle density of $\sim 10^8/\mathrm{cm}^3$ for both species, though we have noticed that the antiproton density plays no role in the dominant three-body recombination of two positrons with one antiproton. The longitudinal velocity of e^- is chosen according to a Maxwell-Boltzmann distribution for a low temperature of either 0.85 or 0.3 K, while the transverse velocity in the xy plane is determined by $(\hbar eB)\frac{1}{2}m_e$. The initial antiproton temperature is chosen to be in equilibrium with the electrons, e.g., either 0.85 or 0.3 K. Before being loaded into the e^--$\bar{p}$ mixture, the positrons (e^+) are initially

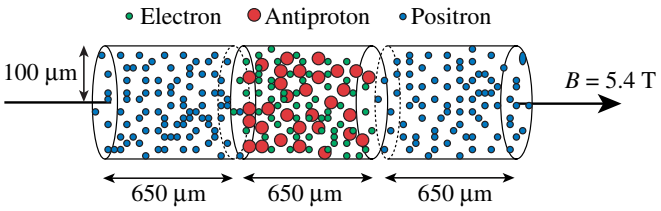

FIG. 1. (Color online) The scheme for our MD simulations of strongly magnetized e^--$\bar{p}$-e^+ plasmas.

*Electronic address: shu@lle.rochester.edu

confined in the same-size side cylinders, as indicated in Fig. 1. We have 8000 e^+'s randomly distributed in each side cylinder, which gives an initial positron density of $\sim 4\times 10^8/\mathrm{cm}^3$. The e^+ temperature is chosen to be $\sim$4.2 K as it is in typical experiments [2]. Thus, we have a total 20 000 particles to simulate. In our simulations, two "mirror" boundary conditions [7] are enforced: (1) a large-mirror boundary (LMB) in which all particles are allowed to move within all three connecting cylinders, and any particles hitting the end edges will be reflected back to the plasma; (2) a small-mirror boundary (SMB) in which only positrons are allowed to move within all cylinders, while e^- and $\bar{p}$ are confined in the middle cylinder.

Since quantum effects are negligible in such dilute plasmas (as the electron de Broglie wavelength is much smaller than the interparticle distance), classical mechanics [4,5,7,8] will be used for our current studies. As it was successfully used for simulations of strongly magnetized e^+-$\bar{p}$ plasmas [7,8], the fourth-order symplectic integrator [13] is also employed for our current modeling of three-component plasmas. More details about the fourth-order symplectic algorithm and its implementation can be found in Ref. [8]. Basically, we treat the long-range Coulomb interaction as a perturbation to the cyclotron motion of the charged particles in the strong magnetic field, unless "close encounters" occur in the low-density plasmas. In this scheme, each time step consists of two stages ("drift" and "kick"). The two stages of action are elegantly combined by some magic numbers [8,13], which gives an accuracy up to $(\Delta t)^4$. During the drift stage, particle coordinates are propagated according to their cyclotron motion. The time-integrated Coulomb forces, which account for all interparticle interactions, instantaneously change the momentum of each particle as an impulse at the kick stage. If close-encounter collisions happen, the total energy of the system will numerically "jump up." Whenever this occurs, we back up one time step and adopt a much smaller time step to evolve the system, until we bring the total energy back to the conservation range. After the close collision finishes, we may recover the large time step again. Such an adaptive algorithm has been used to maintain the error in energy conservation under 1% of the system energy at all times during the simulations. Moreover, in order to handle a large number ($\sim$20 000) of particles in our MD simulations, we have implemented the fourth-order symplectic integrator by the message-passing-interface parallelization scheme, with the decomposition of particles. In this way, we can run such large-scale simulations on state-of-the-art supercomputers up to a time scale of microseconds.

Before allowing the positrons to go into the e^--$\bar{p}$ clouds, any potential heating in the e^--$\bar{p}$ mixture is checked by letting them evolve alone for $\sim$0.5 μs. The MD simulations with the SMB condition indicate that the antiprotons can actually be kept as cold as the electrons for a long time. Although one may dump out the electrons before loading positrons in experiments, we speculate that the electrons may affect the recombination of e^+-$\bar{p}$ if they are kept in the Penning trap. One effect might be that the simultaneously formed positroniums may increase the antihydrogen-production (three-body-recombination) rate, since they have a larger cross section of collision with antiprotons. We therefore include these cold electrons in our MD simulations. Letting the positrons mix with the ultracold e^--$\bar{p}$ clouds, we simulate such systems in both LMB and SMB conditions. Recombinations among e^--e^+ and e^+-$\bar{p}$ are clearly observed, which generate positronium and antihydrogen atoms, respectively. Similar to what we did before for $\bar{\mathrm{H}}$ atoms [7,8], we identify these recombinations by calculating the minimum distance of e^--e^+ and e^+-$\bar{p}$ pairs. If both particles stick together for a certain amount of time (e.g., $>$50 ns for $\bar{\mathrm{H}}$ and $>$25 ns for Ps), such a pair is taken as a recombined Ps or $\bar{\mathrm{H}}$ atom, which will be used for further analysis of their properties.

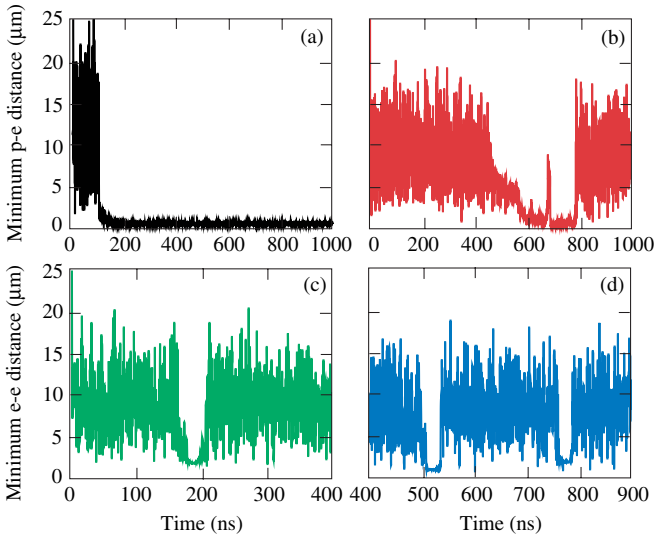

FIG. 2. (Color online) The minimum distance between a $\bar{p}$ and its nearest e^+ is plotted as a function of time in (a) and (b), while the cases for e^--e^+ pairs (positroniums) are shown in (c) and (d).

We start presenting our results from a SMB simulation with an initial e^--$\bar{p}$ temperature of 0.3 K. In Fig. 2, we plot the minimum distance between a $\bar{p}$ and its nearest e^+ as a function of time, for two representative $\bar{\mathrm{H}}$ atoms in Figs. 2(a) and 2(b); while the cases for positroniums (e^--e^+ pairs) are drawn in Figs 2(c) and 2(d). From Fig. 2(a), we observe that the minimum $\bar{p}$-e^+ distance varies rapidly and irregularly from 1.5 to 25 μm during the first 0.15 μs; it then exhibits regular oscillations from t=0.15 to 1.0 μs. Checking the particle index of the sticking e^+, we find that it does not change from t=0.15 to 1.0 μs. Thus, such a regular oscillation clearly indicates the recombination of an e^+ with a $\bar{p}$, i.e., an $\bar{\mathrm{H}}$ atom is formed. Figure 2(b) shows more details of another $\bar{\mathrm{H}}$ formation process, in which the three-body dynamics exhibits itself. The distinct spike of the minimum e^+-$\bar{p}$ distance around t=700 ns in Fig. 2(b) illustrates that the other e^+ takes off when one e^+ approaches and binds to the $\bar{p}$. The formed $\bar{\mathrm{H}}$ atoms have their own lifetime in the plasmas. They can be destroyed by collisions, which is also exemplified in Fig. 2(b) (the $\bar{\mathrm{H}}$ atom is destroyed at around t=800 ns). In contrast to $\bar{\mathrm{H}}$ atoms, positroniums have much shorter lifetimes due to their light mass. This has been shown in Figs. 2(c) and 2(d), in which we see some e^--e^+ recombinations

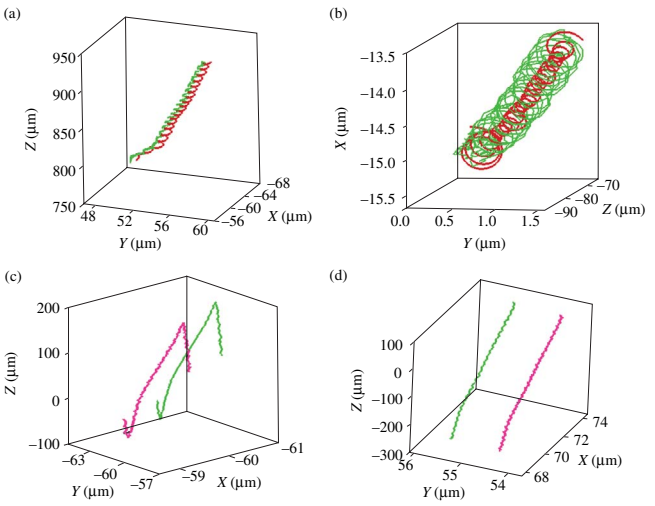

FIG. 3. (Color online) The trajectories for some recombined $\bar{H}$ atoms (a), (b) and positroniums (c), (d). The $\bar{p}$ and e^- are plotted as black (red) lines, while e^+'s are indicated by gray (green) lines.

for a short time (~30 ns). Since they are "quickly" moving around inside the plasma, the positroniums can be easily destroyed and recombined again, as indicated in Fig. 2(d).

To further explore the dynamical motion of the recombined particle pairs, we plot the detailed trajectories of some representative $\bar{H}$ atoms and positroniums in Fig. 3. Figures 3(a) and 3(b) represent some formed antihydrogen atoms, while Figs. 3(c) and 3(d) are for positroniums. From Figs. 3(a) and 3(b), we find that the positrons (gray/green line) are coincidently moving with the antiprotons (black/red line). In addition to their own cyclotron motion, they "orbit" each other and move together for more than 100 μm [Fig. 3(a)] along the magnetic field in the plasma. For the positroniums shown in Figs. 3(c) and 3(d), however, the pairs of e^--e^+ are moving only parallel to each other. They are actually stabilized by the aid of the strong magnetic field to form a "giant-dipole" type of positronium. All positroniums identified in our simulations are of this giant-dipole type. It is not yet clear to what extent the existence of these positroniums increases the possibility of $\bar{H}$ formation in our simulations. However, we find apparent evidence that an electron aids the recombination of an e^+ with a $\bar{p}$. In general, antihydrogen atoms can be formed in such strongly magnetized, three-component plasmas via the two three-body channels $e^+ + e^+ + \bar{p} \rightarrow \bar{H} + e^+$ and $e^- + e^+ + \bar{p} \rightarrow \bar{H} + e^-$.

Besides performing the 0.3 K modelings for both SMB and LMB conditions, we have also performed an MD simulation for the e^--$\bar{p}$ temperature of 0.85 K using the small-mirror boundary condition. As described above, 20 000 particles (including 16 000 e^+, 2000 e^-, and 2000 $\bar{p}$) are used for all simulations. Using our criteria for recombination (i.e., sticking time larger than 50 ns), we have identified a total of 16, 13, and 10 $\bar{H}$ recombination events during the 1 μs simulation time, respectively, for the three cases 0.3 K (SMB), 0.3 K (LMB), and 0.85 K (SMB). The 0.3 and 0.85 K temperatures are given for the initial e^--$\bar{p}$ mixture. The analyses

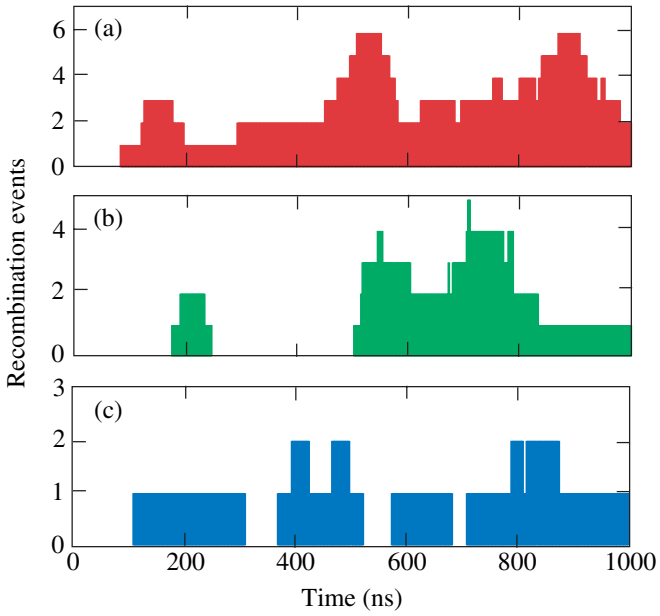

FIG. 4. (Color online) The time dependence of $\bar{H}$ recombination for three MD simulations: (a) 0.3 K (SMB), (b) 0.3 K (LMB), and (c) 0.85 K (SMB).

of $\bar{H}$ atom properties are made for these identified recombination events. We show the results in Figs. 4 and 5. To investigate the temporal behavior of $\bar{H}$ formation during the whole time of plasma evolution, we plot the recombination events against time for these three cases (Fig. 4). It is seen that the recombination starts to appear sooner or later after 0.1 μs mixing of e^+ with the e^--$\bar{p}$ clouds. The oscillation of $\bar{H}$ events with time manifests the competition between re-

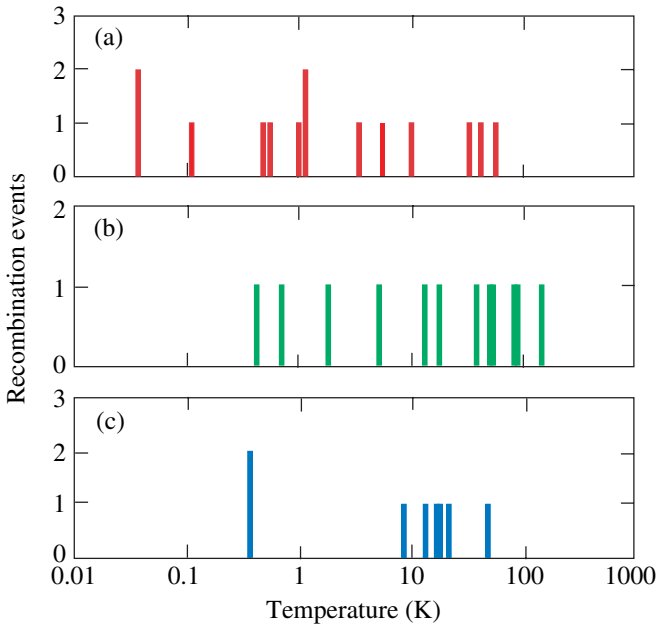

FIG. 5. (Color online) The temperature distribution of the formed $\bar{H}$ atoms for the same MD simulations as in Fig. 4: 0.3 K (SMB) (a), 0.3 K (LMB) (b), and 0.85 K (SMB) (c).

combination and collision (destruction) of the e^+-$\bar{p}$ pairs. It seems that the 0.3 K (SMB) condition [Fig. 4(a)] gives not only more $\bar{H}$ atoms but also a more stable $\bar{H}$ formation than the other two cases.

Finally, Fig. 5 shows the temperature analysis of these formed $\bar{H}$ atoms for the same simulation cases. Note that since we are plotting the $\bar{H}$ temperature in a logarithmic scale, some of the histograms for close temperature points are overlapped in the high-temperature region. Basically, we calculate the center-of-mass (c.m.) kinetic energy for the recombined pairs of e^+-$\bar{p}$. The time averaging of the c.m. energy was done for the lifetime of individual $\bar{H}$. This quantity tells us how fast the recombined antihydrogen atoms are moving inside the plasma. It may, therefore, be associated with a "temperature" for these formed $\bar{H}$ atoms ($E_{\text{c.m.}} \sim kT$). It is very interesting to find from Fig. 5 that a certain number of antihydrogen atoms are really produced at a temperature below $\sim$1 K. Some of them are even as ultracold as $\sim$38 mK, as indicated in Fig. 5(a). Unlike the hot mixing cases [6–9] in which the $\bar{p}$ temperature is always higher than that of e^+, our current cold mixing simulations show that the formed $\bar{H}$ atoms generally have a scattered temperature distribution. That is, we no longer have a distinct signature of the initial $\bar{p}$ temperature in the $\bar{H}$ temperature distribution, as it may have been washed out by the hot positrons. For the SMB simulations [Figs. 5(a) and 5(c)], an appreciable portion of these formed $\bar{H}$ atoms are driven below the initial $\bar{p}$ temperatures during the three-body recombinations. For the LMB simulation depicted by Fig. 5(b), however, we find that all $\bar{H}$ atoms have temperatures higher than that of the initial antiprotons. Also, the LMB simulation results in a higher $\bar{H}$ temperature above $\sim$100 K. This may be attributed to the fact that in the LMB condition the electrons are allowed to leave the antiproton region, so that $\bar{p}$ may be heated up during the time when electrons fly away under the Coulomb repulsion of antiprotons. Nevertheless, in this case we still obtain some ultracold antihydrogen atoms ($<$1 K). In general, the confinement of the e^--$\bar{p}$ clouds during the e^+ mixing (SMB) gives not only more but also colder $\bar{H}$ atoms.

In summary, it has been realized that making ultracold antiprotons is of crucial importance for producing ultracold antihydrogen atoms. We propose that ultracold-electron sources, which are obtainable in experiments, may be used as the coolant for further antiproton cooling. By properly assuming that antiprotons can be brought to thermal equilibrium with the coldest electrons in a Penning trap, we have performed large-scale MD simulations for mixtures of cold positrons with such ultracold electron-antiproton clouds. Although the absolute recombination events are not many from our simulations and the plasma rotation effects may limit the number of particles to certain values, we anticipate that more $\bar{H}$ atoms can be added in experiments, as the recombination events roughly scale with the number of particles involved. Nevertheless, the simulation results elucidate that a certain portion of antihydrogen atoms are produced at a very low temperature below $\sim$1 K, which may be trapped in a somewhat low magnetic field [12]. This may lead to further critical investigations on both the decay dynamics and possible manipulations of these high-Rydberg $\bar{H}$ atoms.

The author acknowledges Dr. Daniel Vrinceanu for useful discussions. This work was partially supported by the U.S. Department of Energy at Los Alamos National Laboratory.

[1] G. Gabrielse, Adv. At., Mol., Opt. Phys. **45**, 1 (2000); M. Niering *et al.*, Phys. Rev. Lett. **84**, 5496 (2000); R. Bluhm, V. A. Kostelecky, and N. Russell, Phys. Rev. D **57**, 3932 (1998); G. Gabrielse, Hyperfine Interact. **44**, 349 (1988).

[2] M. Amoretti *et al.*, Nature (London) **419**, 456 (2002); G. Gabrielse *et al.*, Phys. Rev. Lett. **89**, 213401 (2002); **89**, 233401 (2002).

[3] G. Gabrielse *et al.*, Phys. Rev. Lett. **93**, 073401 (2004); C. H. Storry *et al.*, *ibid.* **93**, 263401 (2004);

[4] S. G. Kuzmin and T. M. O'Neil, Phys. Rev. Lett. **92**, 243401 (2004); D. Vrinceanu *et al.*, *ibid.* **92**, 133402 (2004); S. G. Kuzmin, T. M. O'Neil, and M. E. Glinsky, Phys. Plasmas **11**, 2382 (2004).

[5] F. Robicheaux and J. D. Hanson, Phys. Rev. A **69**, 010701(R) (2004); F. Robicheaux, Phys. Rev. A **70**, 022510 (2004); E. M. Bass and D. H. E. Dubin, Phys. Plasmas **11**, 1240 (2004);

[6] M. Amoretti *et al.*, Phys. Rev. Lett. **91**, 055001 (2003); Phys. Lett. B **583**, 59 (2004).

[7] S. X. Hu *et al.*, Phys. Rev. Lett. **95**, 163402 (2005).

[8] D. Vrinceanu *et al.*, Phys. Rev. A **72**, 042503 (2005).

[9] N. Madsen *et al.*, Phys. Rev. Lett. **94**, 033403 (2005).

[10] G. Gabrielse *et al.*, Phys. Rev. Lett. **63**, 1360 (1989); Phys. Lett. B **548**, 140 (2002); M. Amoretti *et al.*, Nucl. Instrum. Methods Phys. Res. A **518**, 679 (2004); N. Kuroda *et al.*, Phys. Rev. Lett. **94**, 023401 (2005).

[11] B. D'Urso, B. Odom, and G. Gabrielse, Phys. Rev. Lett. **90**, 043001 (2003).

[12] W. Bertsche *et al.*, Nucl. Instrum. Methods Phys. Res. A **566**, 746 (2006).

[13] H. Yoshida, Phys. Lett. A **150**, 262 (1990).